




## Buck-Based Photovoltaic Microinverter Coupled to a Discharge Circuit

Mohammed El Bachir Ghribi<sup>1</sup>, Zine Eddine Touhami Ternifi<sup>2</sup>, Ghalem Bachir<sup>2</sup>, Michel Aillerie<sup>3</sup>  
1- Applied Power Electronics Laboratory (LEPA), University of science and technology of Oran Mohamed Boudiaf, Oran, Algeria.

Email: mohammedelbachir.ghribi@univ-usto.dz (Corresponding author) 

2- Laboratory of sustainable development of the electrical energy (LDDEE), University of science and technology of Oran Mohamed Boudiaf, Oran, Algeria.

Email: touhamyz@yahoo.fr, ghalem.bachir@univ-usto.dz

3- Laboratoire Matériaux Optiques, Photonique et Systèmes (LMOPS), Université de Lorraine, CentraleSupélec, F-57000 Metz, France.

Email: michel.aillerie@univ-lorraine.fr

### ABSTRACT:

The aim of this paper is to introduce a novel microinverter design that is based on the DC/DC converter, Buck. This structure is intended to provide a sinusoidal voltage to low-power autonomous loads embedded in vehicles, which require excellent waveform quality. In the first part, the paper presents the new topology, its modeling, and the control strategies employed. Two control strategies are discussed, including the classical control with a PI regulator and the sliding mode control with the step function. The dimensioning is carried out using the Ziegler-Nichols method, and the stability is ensured using the Lyapunov method. In the second part, the paper comments on the results obtained from different simulations in terms of harmonic distortion (THD), efficiency and control robustness with different sources, such as battery and photovoltaic panel.

**KEYWORDS:** Micro-inverter, Buck, Discharge circuit, Lyapunov method.

### 1. INTRODUCTION

Researchers are currently dedicating significant efforts to improving photovoltaic inverters and their architectures. Over the past decades, their work has primarily focused on increasing the conversion efficiency and reliability of micro-inverters by developing increasingly robust topologies that use fewer power electronics components. Micro-inverters enable each panel to directly provide a sinusoidal voltage to either power a direct load or be integrated into the distribution electrical grid. Micro-inverters appear as many times as there are panels and are generally sized to be integrated with a specific type of panel with a certain voltage, power, and current. They provide a standardized output voltage, already pre-sized. Micro-inverter technology must be as simple as possible while ensuring high conversion efficiency and reliability. Additionally, their individual cost must be kept as low as possible while guaranteeing good quality of output voltage and current.

Among the requirements imposed on the micro-inverter are also a output voltage waveform with low THD, a fast transient response, and the minimization of errors in steady-state operation.

Most existing micro-inverter topologies use a multi-stage structure, typically two stages. In the vast majority of cases, the first stage is a DC/DC converter placed upstream of an inverter bridge that constitutes the second stage. The first stage's role is to pre-shape the waveform of voltage and current, providing a rectified sinusoidal waveform voltage. This rectified sinusoidal waveform is then modulated with the inverter bridge using a 180° phase shift to obtain a

©The Author(s) 2024

Paper type: Research paper

<https://doi.org/10.30486/mjee.2024.1992377.1189>

Received: 27 October 2023; revised: 19 December 2023; accepted: 25 January 2024; published: 1 March 2024

How to cite this paper: M. El Bachir Ghribi, Z. E. Touhami Ternifi, Gh. Bachir, M. Aillerie, “**Buck-Based Photovoltaic Microinverter Coupled to a Discharge Circuit**”, *Majlesi Journal of Electrical Engineering*, Vol. 18, No. 1, pp. 323-333, 2024.

sinusoidal voltage. Among the most used DC/DC converters are boost and buck-boost converters, as they amplify the voltage from the solar panel or battery to provide an amplified voltage with a higher value [1-8]. The buck converter is also used, but the input voltage must be higher than the maximum value of the output alternating voltage, or a voltage-boosting transformer must be used [9-13]. Converters can also be used to track the maximum power point of solar panels, and the obtained voltage is then directly modulated; this topology is generally coupled with a voltage filter [14-18].

The main proposition of this new microinverter topology is based on the utilization of a buck converter and a discharge circuit as the first stage, where the buck converter's role is to increase the voltage value and the discharge circuit's role is to decrease this voltage. The proper operation of both circuits provides a rectified sinusoidal voltage, whose maximum amplitude is lower of the source, which is either a battery or a photovoltaic panel.

The bridge is controlled with a  $180^\circ$  phase shift at a frequency of 50 Hz to obtain a modulated voltage at the midpoint of the period [12,13]. This paper presents a detailed design of the converter used based on the input and output voltages, as well as a state-space modeling of the first stage of the inverter based on the switch states. This topology does not use any filters, and the maximum switching frequency is limited to 20 kHz.

Two control strategies are used for this topology. The first is linear control with a PI regulator, sized using the Ziegler-Nichols method. The second is non-linear and uses sliding mode control with the Smooth function. Stability analysis is performed using the Lyapunov method, and a comparison is made between the two controllers in terms of THD and voltage ripple.

Two continuous voltage sources are also used for simulations, including a photovoltaic panel model with a maximum power voltage higher than the buck's maximum voltage and a 40V battery.

About the output voltage, its reference is set to 24V, with the goal of having a standard voltage to power fixed or embedded devices such as LED lighting, actuators, electronic components, protection systems, etc. If necessary, this voltage can be increased using a boost transformer. This new micro-inverter topology has the advantage of using a reduced number of components while ensuring good performance in terms of harmonic distortion rates. It consists of two high-frequency power switches, limited to 20 kHz by the control, as well as four low-frequency switches operating at 50 Hz. It also includes a diode, a capacitor, and two coils.

## 2. PROPOSED TOPOLOGY

In the suggested configuration, when switch K1 of the buck converter is activated, the capacitor begins to charge, and the voltage across it increases (in accordance with equation 1). When the buck converter switch is blocked, the capacitor starts to discharge through the load and the discharge circuit (this phase is represented by equation 4). The combination of these two phases allows for the creation of any form of DC voltage. Thus, effective control of this cycle generates a rectified sinusoidal voltage at the output of the buck.

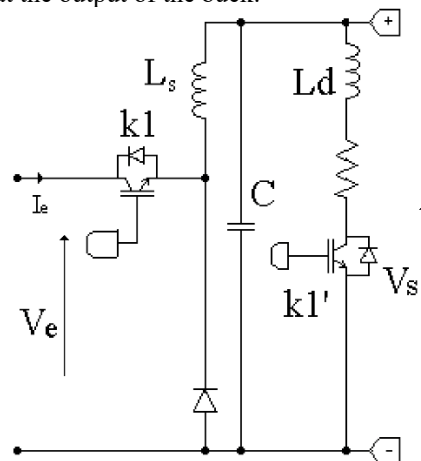


Fig. 1. Diagram of the Buck converter with the discharge circuit.

In this configuration, the discharge inductance denoted as  $L_d$  is used to limit the current of circuit when switch  $K1'$  is activated, to prevent any deterioration of the switch and to smooth the voltage, in addition to limiting the switching frequency. The inverter is powered either by a battery or a photovoltaic panel, chosen to ensure a maximum continuous voltage equal to or greater than  $24\sqrt{2}$  V, with the control reference voltage noted as  $V_{ref}=24\sqrt{2}.\sin(2\pi 50t)$  [4], resulting in an effective value of 24 V.

The rectified sinusoidal waveform allows the four switches of the inverter bridge to switch at a frequency of 50 Hz.

The rated power consumed by the chosen load is 150 W. To evaluate the response of the control and topology, a test with a inductive load.

**2.1. Modelling the Buck with a discharge circuit.**

The system is modeled using a state-space representation that incorporates the state of switch k1 with the help of a Boolean variable (S). If k1 is blocked, S=0; otherwise, S=1. The variable S also represents the state of the control signal S that governs k1, which is the inverse of the control signal that governs k1' [19].

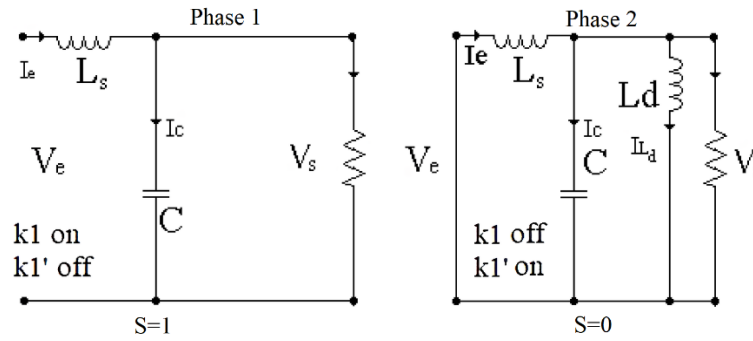


Fig. 2. Buck equivalent diagram with discharge circuit.

**Phase 1**

Switch k1 is on and k1' is blocked.

$$\frac{dV_s}{dt} = \frac{I_e}{C} - \frac{V_s}{RC} \tag{1}$$

$$\frac{dI_e}{dt} = -\frac{V_s}{L_s} + \frac{V_e}{L_s} \tag{2}$$

$$\frac{dI_{Ld}}{dt} = 0 \tag{3}$$

**Phase 2**

The switch k1 is blocked and k1' is on, the diode is on, which gives the equivalent diagram in Fig. 2.

$$\frac{dV_s}{dt} = \frac{I_e}{C} - \frac{I_{Ld}}{C} - \frac{V_s}{RC} \tag{4}$$

$$\frac{dI_e}{dt} = -\frac{V_s}{L_s} \tag{5}$$

$$\frac{dI_{Ld}}{dt} = \frac{V_s}{L_d} \tag{6}$$

The introduction of the switch state the result is as follows:

$$\frac{d}{dt} \begin{bmatrix} V_s \\ I_e \\ I_{Ld} \end{bmatrix} = \begin{bmatrix} \frac{-1}{RC} & \frac{1}{C} & \frac{1-S}{C} \\ \frac{-1}{L_s} & 0 & 0 \\ \frac{1-S}{L_d} & 0 & 0 \end{bmatrix} \cdot \begin{bmatrix} V_s \\ I_e \\ I_{Ld} \end{bmatrix} + \begin{bmatrix} 0 \\ \frac{S}{L_s} \\ 0 \end{bmatrix} V_e \tag{7}$$

This model is not perfectly representative in case of a strongly inductive load, if S=1, the representation becomes of order two.

$$A = \begin{bmatrix} \frac{-1}{RC} & \frac{1}{C} \\ \frac{-1}{L_s} & 0 \end{bmatrix}, B = \begin{bmatrix} 0 \\ 1 \\ L_s \end{bmatrix} \quad (8)$$

## 2.2. Dimensioning

The capacitor in a buck converter serves the purpose of supplying current to the load during the phase when the source is disconnected (phase 2). The capacitor's capacity is calculated to ensure the supply of the nominal current to the load for one quarter of the reference voltage period (as indicated by equation 9). It's important to note that the value of this capacitance is directly related to the reference voltage. If the reference voltage of the buck converter is lower, the required capacitance increases, as it needs to provide a higher current, resulting in more losses for undersized loads.

$$C_{\max} = \frac{I_c \Delta t}{\Delta V} = \frac{I_c}{4 f_s \Delta V} \approx -\frac{I_{s-\max}}{2 \pi f_s \Delta V} \quad (9)$$

The discharge inductance plays a crucial role in limiting the current of the discharge circuit. It is sized to ensure that the maximum discharge current is not exceeded, especially when the frequency is at its minimum. For this circuit, the control signal frequency is bounded between 2 and 20 kHz, and equation 10 provides the formula for sizing the discharge inductance.

$$L_d < \frac{V_{s-\max}}{I_{Ld-\max} * f_{com-\min}} \quad (10)$$

In addition to using an inductance to regulate the current of discharge circuit, it is also conceivable to incorporate a resistor, either in series with the inductance or independently. When utilizing a photovoltaic source, the input inductance can be considered negligible, given that the panel voltage follows the buck output voltage ( Fig. 6). However, for the battery, the input inductance is essential and is proportional to the difference between the battery voltage and the buck converter voltage, as formulated in equation (11).

$$\frac{V_e - V_{s-\max}}{I_{s-\max} * f_{com-\min}} < L_s < \frac{V_{s-\max}}{I_{s-\max} * f_{com-\min}} \quad (11)$$

## 2.3. Classic control with PI controller.

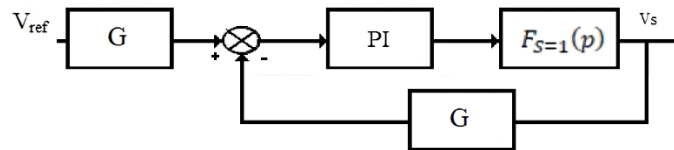


Fig. 3. Control loop S=1 with PI corrector.

The control is executed using a classical Proportional-Integral (PI) controller, as shown in Fig. 3. The sizing of the controller is carried out using the Ziegler-Nichols open-loop method, for the transfer function obtained with the switch state k1 on (S=1), as given by equation (12).

$$F_{S=1} = \frac{\frac{1}{L_s C}}{s^2 + \frac{1}{RC} s + \frac{1}{L_s C}} \quad (12)$$

The Ziegler-Nichols open-loop approach is a practical technique used to adjust the parameters of a PID controller in the field of electrical engineering. This method includes introducing a disturbance to the system and analyzing the open-loop response to ascertain the appropriate values for the controller coefficients [19-21].

$$K_p = \frac{0.9 \cdot \Delta Y}{G \cdot P \cdot L} = \frac{0.9 \cdot t_u}{G \cdot L}, \quad K_i = 3.33 \frac{L}{G} \quad (13)$$

To generate the control signal and prevent surpassing the maximum switching frequency, the output of the controller is systematically compared with  $V_{ref}$  signal. This comparison enables the creation of a suitable control signal, ensuring its application to the system is well-regulated.

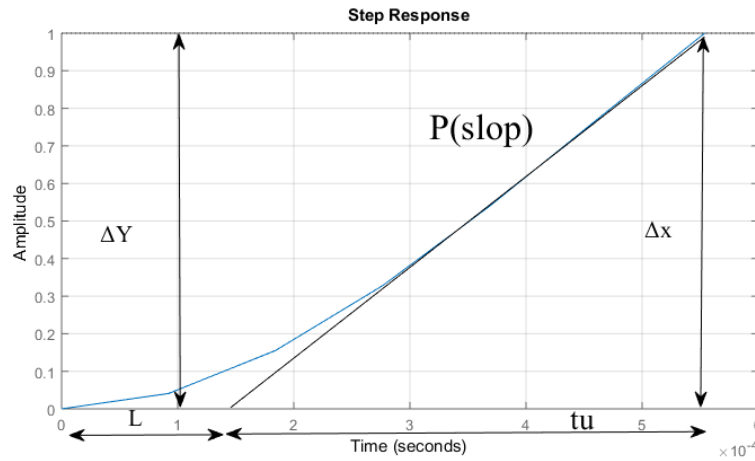


Fig. 4. Rethinking the system at a step (S=1).

**2.4. Sliding mode control and its stability.**

The second control device employs sliding mode control to adjust the inverter's operation, as detailed in references [22-24]. In this configuration, the step function is chosen due to the non-linearity of the system and its transitions between two states, thereby avoiding the addition of any additional oscillation to the existing signal.

$$S = step(\varepsilon) \quad (14)$$

The control's sliding surface is naturally defined as the error in the output voltage of the buck converter. Stability analysis of this control scheme employs the Lyapunov method, renowned for assessing global or partial stability of dynamic systems. This method relies on an energy function, typically quadratic, to evaluate stability of equilibrium points or motion. In our case, it's applied to a nonlinear system oscillating between two states. For stability, the Lyapunov function must be zero at the origin, strictly positive elsewhere, and its derivative must be strictly negative. Equation (15) defines the chosen function. We assume the switching frequency significantly exceeds that of the inverter, enabling us to consider the buck converter's reference voltage as constant[25-28].

$$V(\varepsilon) = \frac{\varepsilon^2}{2} \quad (15)$$

Equation 16 illustrates that the variation in the error is consistently proportional to the inverse of the change in the output voltage.

$$\varepsilon = V_{ref} - V_s \rightarrow \frac{d\varepsilon}{dt} = -\frac{dV_s}{dt} \quad (16)$$

**Phase 1** The error is positive the switch k1 becomes conductive the capacitance is charged which causes the voltage to increase, as shown in eq 1.

$$I_e > \frac{V_s}{R} \quad (17)$$

$$\varepsilon > 0 \rightarrow S = 1 \rightarrow \frac{dV_s}{dt} > 0 \rightarrow \frac{d\varepsilon}{dt} < 0 \quad (18)$$

**Phase 2** If the error is negative, the discharge circuit switch is turned on and the capacitance discharges, leading to a decrease in voltage, as shown in eq 4.

$$I_e < I_{Ld} + \frac{V_s}{R} \quad (19)$$

$$\varepsilon < 0 \rightarrow S = 0 \rightarrow \frac{dV_s}{dt} < 0 \rightarrow \frac{d\varepsilon}{dt} > 0 \quad (20)$$

The drift of the Lyapunov function is strictly negative for both phases, it indicates that the energy of the system is decreasing over time, ensuring that the system is stable. Therefore, it can be concluded that the control is stable for the entire system.

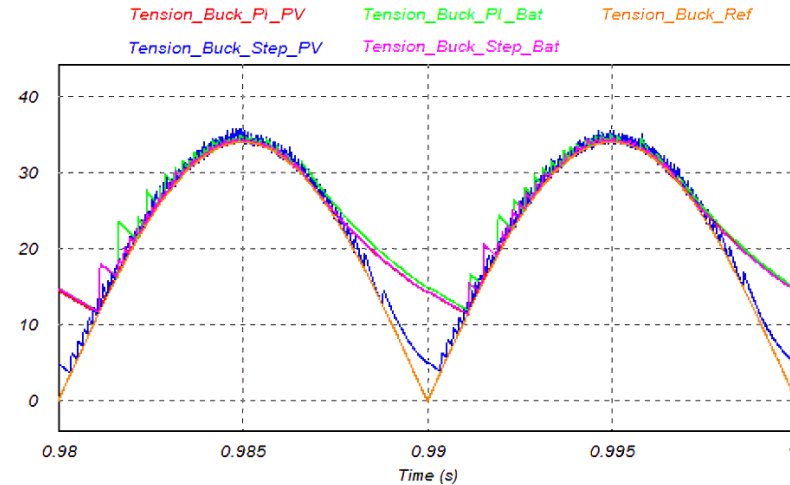
$$V(0) = 0; V(\varepsilon) = \frac{\varepsilon^2}{2}, \varepsilon \neq 0; V'(\varepsilon) = \varepsilon' \varepsilon < 0 \quad (21)$$

### 3. RESULT AND DISCUSSION

The inverter is designed to generate a current of 6 A at a voltage of 24 V, resulting in a total power output of 150 W. The performance evaluation of the two regulators is conducted through various tests using different energy sources. Two sources are employed for these tests: a photovoltaic panel with an open-circuit voltage of 44 V and a maximum power voltage of 36 V. The second source is a 40 V battery.

#### 3.1. Without Discharge Circuit.

In the absence of the discharge circuit, the output response of the buck converter is significantly affected by both the power source's characteristics and the dimensions of the converter. Consequently, the capacitance fails to discharge completely, resulting in the absence of a zero crossing.



|                                | THD 50 Hz | RMS    |
|--------------------------------|-----------|--------|
| Buck voltage PI photovoltaic   | 18 %      | 25.3 V |
| Buck voltage Step photovoltaic | 5 %       | 24.7 V |
| Buck voltage PI Battery        | 19 %      | 25.9 V |
| Buck voltage Step Battery      | 18.5 %    | 25.4 V |
| Buck voltage Reference         | 0.09 %    | 24 V   |

Fig. 5. Buck voltage output without discharge circuit.

Fig. 5 indicates that among the four test results without the discharge circuit, the sliding mode regulator with the photovoltaic panel exhibits the best performance, with a harmonic distortion rate (THD) of 5%. In contrast, the other three test results show a very high THD, exceeding 18%, suggesting that the buck converter alone should be designed to handle a constant nominal load rather than a variable load under such conditions

#### 3.2. With the Use of the PI Regulator.

The results of the micro-inverter demonstrate satisfactory performance, producing a sinusoidal output with a THD of less than 2% for both current and voltage. The integration of the discharge circuit facilitates zero crossing at  $t = \{0, T/2\}$  when the inverter bridge switches are toggled, as illustrated in Fig. 6.

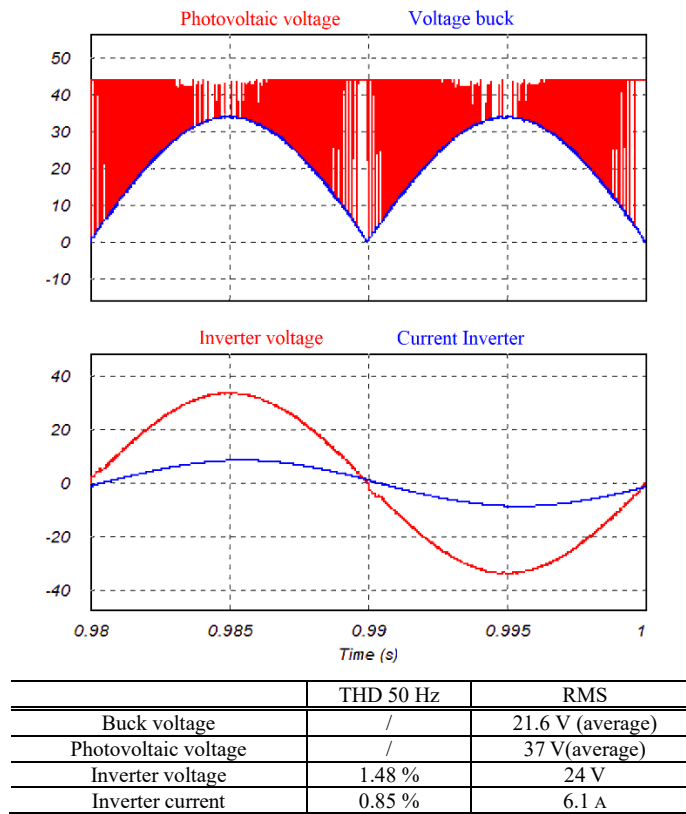


Fig. 6. Inverter output with a PV source and PI corrector.

The voltage output of the inverter, powered by a photovoltaic source, is illustrated in Fig. 6. An important aspect is that the panel voltage follows that of the capacitor during the activation of the switch k1. During this phase, the capacitance charges, thereby increasing the voltage. When k1 is deactivated, the panel voltage returns to its open-circuit value, and the capacitor discharges either through the load or via the discharge circuit. This results in a decrease in the voltage of the buck converter. The harmonic distortion rate of the current is excellent, equivalent to 0.85%.

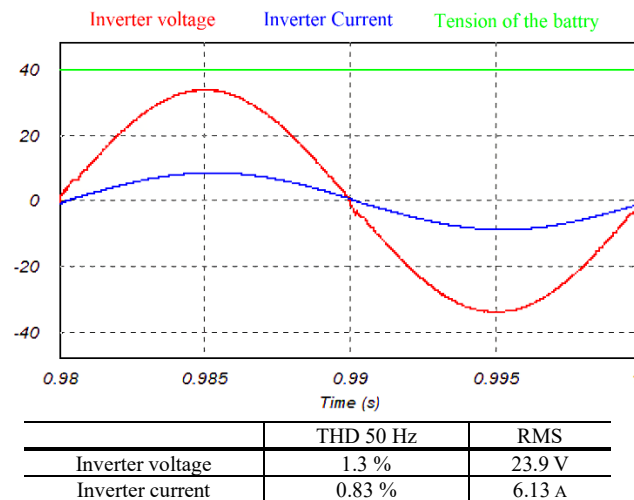


Fig. 7. Inverter output with Battery as source and PI corrector.

The transition from the photovoltaic panel to a battery yields comparable results, with the same harmonic distortion and root mean square (RMS) values. This highlights the robustness of the micro-inverter against variations in the input

source. The results are summarized in Fig. 7.

3.3. With the Use of the Step Function.

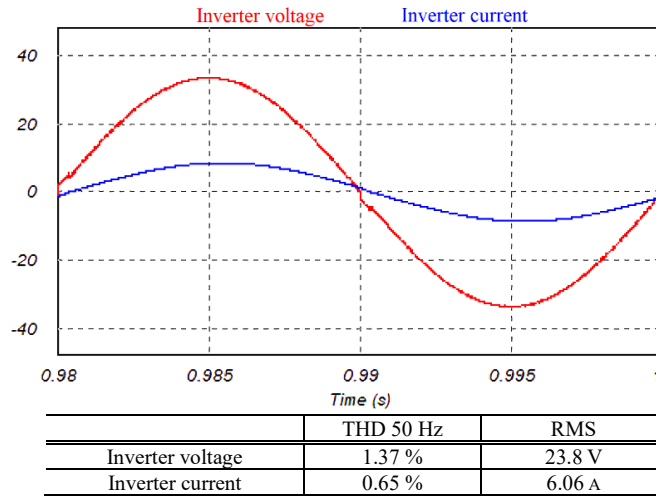


Fig. 8. Inverter output with PV source using the step function.

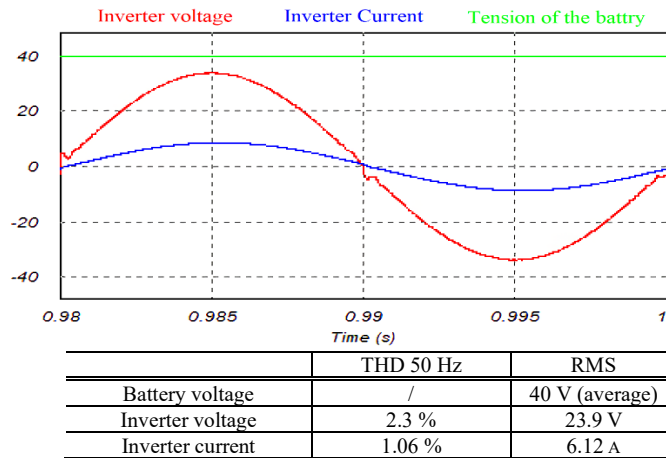


Fig. 9. Inverter output with Battery as source using the step function.

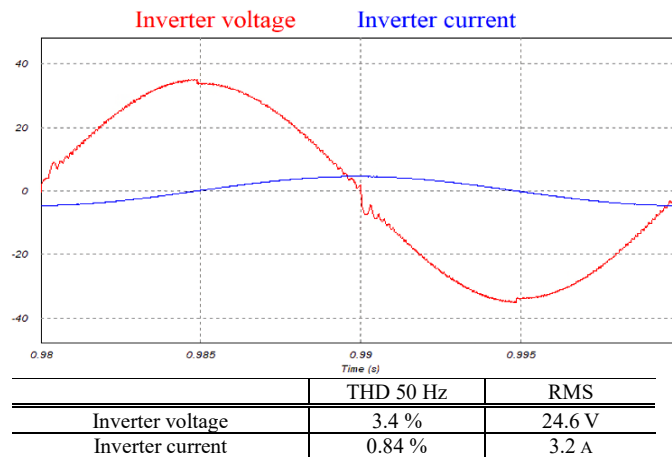


Fig. 10. Test with purely inductive load.



The inverter performance in the case of a photovoltaic source is slightly improved with sliding mode control compared to conventional control, resulting in a current THD of less than 0.7% provided by the inverter. However, the inverter voltage waveform exhibits a less favorable THD, especially in terms of voltage, due to a less precise zero-crossing transition during the inverter bridge switching moments. Despite this, the overall result remains acceptable.

Inverter sizing is based on the assumption of a resistive load, meaning that a highly inductive load can disturb the voltage, and to maintain high power quality, the current supplied by the inverter must be reduced to half its nominal value for a purely inductive load. Fig. 10 illustrates this degradation of inverter voltage to 3 %, while the current is not disturbed with a THD of less than 1 %, as demonstrated in Fig. 10.

#### 4. PERFORMANCE EVALUATION

Table 1 highlights that a significant portion of losses remains constant. In the case of undersizing the load, the current flowing through the discharge circuit increases, resulting in a decrease in efficiency. The switching frequency of the buck converter varies from one to three times depending on the switching time, with an average frequency of 10 kHz. The results are presented in Table 1 using a parameter  $\gamma$ , representing the phase of the period, where  $t = \gamma * T$ . The variation is cyclical, with its cycle spanning half of a period.

Table 1. Efficiency (battery) and Switching frequency.

|                           |      |      |       |     |     |      |
|---------------------------|------|------|-------|-----|-----|------|
| Power (W)                 | 25   | 49   | 61    | 81  | 122 | 145  |
| Efficiency (%)            | 60   | 83   | 85    | 88  | 92  | 93   |
| $\gamma$                  | 0.03 | 0.08 | 0.013 | 0.2 | 0.3 | 0.45 |
| Switching frequency (kHz) | 6    | 11   | 14    | 12  | 10  | 6    |

In Fig. 11a, it is observed that the rise in reactive power provided by the inverter correlates directly with the degradation of voltage harmonic distortion. This degradation primarily stems from the fact that at instants  $t = \{0, T/2\}$ , the current peaks, causing the buck voltage to increase too rapidly compared to the reference. Furthermore, the beat is also more pronounced, as depicted in Fig. 10. However, the current exhibits greater resilience to load variations, maintaining a range between 0.6% and 1.4%, (Fig. 11b).

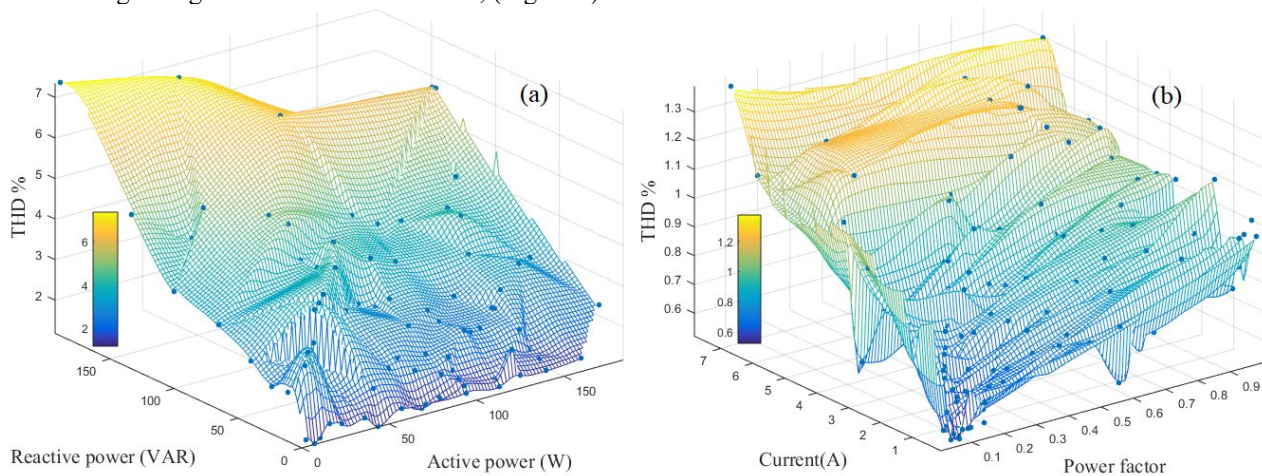


Fig. 11. a) THD of the inverter voltage, b) THD of the inverter current.

The maximum power transmitted to the buck converter from a solar panel is proportional to the duty cycle, and the maximum duty cycle is  $2/\pi$ . For a load of 150 W, the maximum power of the panel is 280 W.

The comparison between the different structures of micro-inverters mentioned in this document reveals significant similarities. The first concerns the use or non-use of voltage and current filters to improve the waveform. The proposed structure directly provides a sinusoidal voltage, thus avoiding the inconvenience of using a filter.

Most of these inverters provide a voltage with a harmonic distortion rate of less than 5%, which is the accepted limit for grid injection. The proposed micro-inverter has a THD of 1.48%. Topologies that offer better results either require a much more complex control to implement or use a filter and a larger number of switches.

Regarding efficiency, in the vast majority of cases where it is provided, it is higher than 90%. The result obtained for this topology is 93%, on average compared to other topologies.

Table 2. Comparison between microinverter structures.

| Reference | Voltage filter | Controlled switches | THD   | Efficiency |
|-----------|----------------|---------------------|-------|------------|
| [1]       | yes            | 5                   | /     | /          |
| [2]       | no             | 4                   | <2%   | 98% <      |
| [3]       | yes            | 6                   | /     | /          |
| [4]       | no             | 5                   | /     | 95% <      |
| [5]       | oui            | 8                   | 2.58% | 97.8%      |
| [6]       | oui            | 5                   | 1.78% | /          |
| [7]       | no             | 6                   | 1%    | 94%        |
| [8]       | yes            | 7                   | /     | 94.6% <    |
| [9]       | yes            | 6                   | /     | 90% <      |
| [10]      | yes            | 4                   | /     | 97% <      |
| [11]      | yes            | 8                   | <1%   | 88%        |
| [12]      | no             | 3                   | 2.07% | /          |
| [13]      | no             | 5                   | 6.32% | /          |
| this work | no             | 6                   | 1.48% | 93 %       |

## 5. CONCLUSION

The combination of the buck topology and the discharge circuit proves to be optimal for presetting the voltage upstream of an inverter bridge in the field of electrotechnics. The asymmetric operation of the two switches enables the provision of a voltage in the form of a rectified sinusoidal wave, making it particularly well-suited for supplying low-power embedded systems.

Nevertheless, this topology comes with notable drawbacks, such as limited voltage robustness for highly inductive loads and a high switching frequency of the two switches. On the positive side, it boasts advantages like a THD of the current below 1.4% and a 50 Hz switching frequency for the inverter bridge. The design involves a minimal number of components, comprising two high-frequency switches and four low-frequency switches. In terms of controls, there is no significant difference between the Proportional-Integral (PI) corrector and the step function.

In summary, the buck topology presents itself as a compelling solution for low-power applications where the quality of the output voltage holds paramount importance in the realm of electrical engineering.

**Data Availability.** Data underlying the results presented in this paper are available from the corresponding author upon reasonable request.

**Funding.** There is no funding for this work.

**Conflicts of interest.** The authors declare no conflict of interest.

**Ethics.** The authors declare that the present research work has fulfilled all relevant ethical guidelines required by COPE.



This article is licensed under a Creative Commons Attribution 4.0 International License.

©The Author(s) 2024

## REFERENCES

- [1] V. H. Garcia-Rodriguez, J. H. Perez-Cruz, R. C. Ambrosio-Lazaro, and S. Tavera-Mosqueda, "Analysis of DC/DC Boost Converter–Full-Bridge Buck Inverter System for AC Generation," *Energies*, vol. 16, pp. 2509, 6, 2023.
- [2] S. Danyali, O. Aghaei, M. Shirkhani, R. Aazami, J. Tavoosi, A. Mohammadzadeh, and A. Mosavi, "A New Model Predictive Control Method for Buck-Boost Inverter-Based Photovoltaic Systems," *Sustainability*, vol. 14, iss. 18, 2022.
- [3] L. Wang, C. Liu, and J. Fang, "Design of a Single-Stage Transformerless Buck–Boost Inverter for Electric Vehicle Chargers," *Applied Sciences*, vol. 12, iss. 13, 2022.
- [4] T. Ternifi, G. Bachir, and M. Aillerie, "A single-phase photovoltaic microinverter topology based on boost converter," *Przegląd Elektrotechniczny*, vol. 95, iss. 4, pp. 215–217, 2019.

- [5] M. G. Marangalu, N. V. Kurdkandi, P. Alavi, S. Khadem, H. Tarzami, & A. Mehrizi-Sani, "A New Single DC Source Five-Level Boost Inverter Applicable to Grid-Tied Systems," *IEEE Access*, 2023.
- [6] E. Davaranhagh, E. Babaei, M. Sabahi, & S. Shahmohamadi, "Three PWM based Control Technics for Switched Boost Inverter," *Majlesi Journal of Electrical Engineering*, vol. 17, iss 4, pp. 1–22, 2023
- [7] M. E. B. Ghribi, Z. E. T. Ternifi, G. Bachir, & M. Aillerie, "Micro-Inverter Based On Symmetrical Boost-Discharge Topology For Photovoltaic Energy Source," *Advances In Electrical And Electronic Engineering*, vol.21, iss. 4, 2023
- [8] J. C. Wu, H. L. Jou, W. C. Wu, and C. H. Chang, "Solar Power Generation System With Power Smoothing Function," *IEEE Access*, vol. 10, pp. 29982–29991, 2022.
- [9] H. Hang, W. Liu, H. Ding, and F. Zheng, "Multi-harmonic oscillation and stability analysis of double-input buck/buck-boost inverter," *IET Power Electronics*, vol. 14, iss. 1, pp. 38–50, 2021.
- [10] S. Han and Y. Cho, "Performance Improvement of Dual-Buck Inverter With Mitigating Reverse Recovery Characteristics and Supporting Reactive Power," *IEEE Access*, vol. 10, pp. 36802-36812, 2022.
- [11] D. Chen and G. Wang, "Differential buck DC-DC chopper mode inverters with high-frequency link," *IEEE Transactions on Power Electronics*, vol. 26, iss. 5, pp. 1444–1451, 2011.
- [12] H. H. Tumbelaka, "A Simple Sinusoidal Buck Converter Working as A Single-Phase Grid-Connected Inverter," *International Journal of Industrial Research and Applied Engineering*, vol. 5, iss. 2, 2020.
- [13] G. C. Diyoke, C. U. Ogbuka, and C. M. Nwosu, "A novel control DC-DC-AC buck converter for single-phase capacitor-start-run induction motor drives," *Advances in Electrical and Electronic Engineering*, vol. 17, iss. 2, pp. 87–95, 2019.
- [14] J. Lopez Seguel, S. I. Seleme, and L. M. F. Morais, "Comparison of the performance of MPPT methods applied in converters buck and buck-boost for autonomous photovoltaic systems," *Ingeniare*, vol. 29, iss. 2, pp. 229–244, 2021.
- [15] H. Attia and K. Hossin, "Efficient maximum power point tracker based on neural network and sliding-mode control for buck converters," *Clean Energy*, vol. 6, iss. 5, pp. 716–725, 2022.
- [16] M. A. Qureshi, F. Torelli, S. Musumeci, A. Reatti, A. Mazza, and G. Chicco, "A Novel Adaptive Control Approach for Maximum Power-Point Tracking in Photovoltaic Systems," *Energies*, vol. 16, iss. 6, 2023.
- [17] R. A. Muhammed & D. R. Sulaiman, "Particle Swarm Optimization (PSO) Based MPPT controller Modeling and Design of Photovoltaic Modules," *Majlesi Journal of Electrical Engineering*, vol.16, pp.4, pp.167–175, 2022
- [18] W. Rahmouni, G. Bachir, and M. Aillerie, "A new control strategy for harmonic reduction in photovoltaic inverters inspired by the autonomous nervous system," *Journal of Electrical Engineering*, vol. 73, iss. 5, pp. 310–317, 2022.
- [19] A. S. Samosir, T. Sutikno, and L. Mardiyah, "Simple formula for designing the PID controller of a DC-DC buck converter," *International Journal of Power Electronics and Drive Systems*, vol. 14, iss. 1, pp. 327–336, 2023.
- [20] J. G. Ziegler and N. B. Nichols, "Optimum settings for automatic controllers," *Trans. ASME*, vol. 64, iss. 8, pp. 759–768, 1942.
- [21] D. Upadhyay, M. Ali, M. Tariq, S. A. Khan, B. Alamri, and A. Alahmadi, "Thirteen-Level UXE-Type Inverter With 12-Band Hysteresis Current Control Employing PSO Based PI Controller," *IEEE Access*, vol. 10, pp. 29890–29902, 2022.
- [22] S. Huerta-Moro, O. Martinez-Fuentes, V. R. Gonzalez-Diaz, and E. Tlelo-Cuautle, "On the Sliding Mode Control Applied to a DC-DC Buck Converter," *Technologies*, vol. 11, iss. 2, pp. 33, 2020.
- [23] G. A. Alamdar, & S. Balochian, "Chaos Control of Permanent Magnet Synchronous Generator via Sliding Mode Controller," *In Majlesi Journal of Electrical Engineering*, vol. 13, iss 1.
- [24] Z. T. Sereshki, N. Pariz, & I. Kardan, "New Adaptive Sliding Mode Controller for Depth Control of Autonomous Underwater Robot," *In Majlesi Journal of Electrical Engineering*, vol. 9, iss 3, 2015.
- [25] C. S. T. Dong, H. H. Vo, T. C. Tran, P. Brandstetter, and P. Simonik, "Application of sensorless sliding mode observer in control of induction motor drive," *Advances in Electrical and Electronic Engineering*, vol. 15, iss. 5, pp. 747–753, 2017. ISSN: 1336-1376.
- [26] A. M. Lyapunov, "The General Problem of the Stability of Motion," Taylor and Francis Ltd., London, UK, 1992.
- [27] M. Ates and S. Laribi, "New results on the global asymptotic stability of certain nonlinear RLC circuits," *Turkish Journal of Electrical Engineering and Computer Sciences*, vol. 26, iss. 1, Article 36, 2018.
- [28] S. M. Ghamari, F. Khavari & H. Mollaei, "Lyapunov-based adaptive PID controller design for buck converter," *Soft Comput*, vol.27, pp. 5741–5750, 2023